photonics

MDPI

Article

Trough-Shift Pointer for Weak Measurement with Large Range and High Spectral Resolution

Wenzhao Huang [1,2], Zifu Su [1], Weiqian Zhao [1], Yafei Yu [1,3], Jindong Wang [2,4] and Zhengjun Wei [1,2,*]

[1] Guangdong Provincial Key Laboratory of Nanophotonic Functional Materials and Devices, School of Optoelectronic Science and Engineering, South China Normal University, Guangzhou 510006, China; 2023022312@m.scnu.edu.cn (W.H.)
[2] Guangdong Provincial Key Laboratory of Quantum Engineering and Quantum Materials, School of Optoelectronic Science and Engineering, South China Normal University, Guangzhou 510006, China
[3] Quantum Science Center of Guangdong-Hong Kong-Macao Greater Bay Area, Shenzhen-Hong Kong, International Science and Technology Park, NO. 3 Binglang Road, Futian District, Shenzhen 518045, China
[4] Guangdong Basic Research Center of Excellence for Structure and Fundamental Interactions of Matter, School of Optoelectronic Science and Engineering, South China Normal University, Guangzhou 510006, China
* Correspondence: weizjweizj@126.com

Abstract

Weak measurement enables the amplification of weak physical effects via post-selection and has become an important tool in precision optical metrology; however, conventional schemes based on mean-pointer shifts suffer from response saturation, limited linear range, and stringent stability requirements. Here, we propose and experimentally demonstrate a weak-measurement scheme based on spectral-interference trough shifts, where the zero-intensity points of the post-selected spectrum act as the measurement pointer, establishing an analytical mapping between the trough displacement and the target phase or time delay. Theoretical analysis shows that, under detector resolution limits, the measurement resolution depends solely on the frequency of extinction point and is independent of weak-value singular amplification or bias-phase modulation, thereby maintaining high sensitivity while avoiding pointer saturation. Experiments demonstrate that the trough-shift scheme achieves significantly better agreement between measured and theoretical sensitivities than biased weak measurement and provides a stable linear response without additional bias-compensation structures, reaching a minimum resolvable phase variation at the 10^{-7} level. Moreover, the approach intrinsically supports multi-period traceable measurements and exhibits strong robustness against intensity fluctuations and spectral distortions, offering a promising route toward high-sensitivity, large-dynamic-range, and stable weak measurement-based optical sensing.

Keywords: quantum measurement; weak measurement; weak value amplification; time delay estimation

Check for updates

Received: 28 February 2026
Revised: 24 March 2026
Accepted: 26 March 2026
Published: 30 March 2026

Copyright: © 2026 by the authors. Licensee MDPI, Basel, Switzerland. This article is an open access article distributed under the terms and conditions of the Creative Commons Attribution (CC BY) license.

1. Introduction

Weak measurement (WM), as a fundamental quantum measurement paradigm [1], has attracted sustained interest since its introduction by Aharonov, Albert, and Vaidman in 1988, owing to its unique advantages in quantum foundations, precision parameter estimation, and optical sensing [2–6]. By engineering an ultrastrongly weak interaction between the system and the pointer and performing post-selection on the system, WM

enables minute physical perturbations to be mapped onto observable pointer shifts, thereby achieving parameter estimation beyond conventional sensitivity limits. In recent years, WM has been widely applied to phase and time-delay measurements, frequency-drift detection, and fiber-based and free-space optical sensing and has gradually evolved into an important tool in quantum metrology.

In most existing WM implementations, the pointer is typically chosen as the mean shift in the probability distribution [2], known as standard weak measurement (SWM) [7,8]. This approach infers the parameter of interest from the displacement of the post-selected pointer distribution and, under weak value amplification (WVA), can in principle achieve substantial sensitivity enhancement. Over the past two decades, SWM has been successfully applied to a variety of metrological tasks, including the measurement of small phase shifts [7–10], time delays [11,12], beam deflections [13,14], and even the spin Hall effect of light [15]. However, the mean-based pointer suffers from several intrinsic limitations. First, WVA is effective only in the vicinity of near-orthogonality between the pre- and post-selected states, resulting in an extremely narrow operational phase window [9,16]. Second, the mean response generally exhibits strong nonlinearity and periodicity over extended parameter ranges, leading to saturation or even sign reversal, which compromises the one-to-one correspondence between the measurement outcome and the target parameter [17]. Third, the post-selection success probability varies sharply with the parameter, making it difficult to maintain stable output intensity and signal-to-noise ratio over a wide dynamic range [7]. Collectively, these constraints hinder the direct application of mean-shift-based WM schemes to large-dynamic-range time-delay sensing.

To overcome these limitations, biased weak measurement (BWM) schemes have been proposed. The core idea is to introduce an additional phase bias or modulation structure to lock the operating point within the linear response regime of the weak value, thereby circumventing the nonlinearities near the WVA singular point [18]. Several implementations have been demonstrated, including those employing a precisely controlled phase bias for longitudinal phase estimation [19], adaptive time-varying parameter estimation [20], and phase modulation techniques [10]. Although such approaches partially relax the trade-off between sensitivity and dynamic range, they typically require extra phase compensators, modulation modules, or multi-channel architectures, thereby increasing system complexity and experimental cost while introducing additional sources of instability and calibration error [3,4,10,17]. Consequently, achieving simultaneously high sensitivity and large dynamic range in WM without resorting to complex compensation structures remains an important open problem in both the theoretical and practical development of WM.

More fundamentally, these limitations originate from the fact that conventional WM schemes rely almost exclusively on the mean of the pointer distribution as the estimator while largely neglecting the richer structural information generated by post-selection interference. In practice, WM implementations in the spectral [7,8], temporal [11,12], and spatial [13–15,21,22] domains often produce pronounced interference fringes, multimodal features, and even extinction points in the pointer distribution. These structural features inherently encode valuable information about the system parameters, yet they have not been systematically exploited within existing frameworks. This naturally raises the question of whether one can go beyond the traditional "mean-shift" paradigm and construct new structure-based pointers, thereby overcoming the intrinsic trade-off between dynamic range and resolution in WM.

Motivated by these considerations, we propose and systematically investigate a new WM pointer based on the displacement of spectral interference nulls, termed the trough shift (TS). Both theory and experiment demonstrate that, under weak coupling and appropriate post-selection with a broadband source, the output spectrum develops bimodal or multimodal interference structures featuring stable extinction points or troughs. The

positions of these troughs respond to perturbations of the system parameters with high sensitivity and near-linear dependence, thereby providing an effective alternative to conventional mean-shift pointers. Compared with standard WM, the TS pointer does not rely on weak-value singular amplification and maintains linear response across multiple interference periods, naturally enabling large dynamic-range measurements. Its resolution limit is primarily set by the spectrometer frequency resolution and can exceed that of SWM by several orders of magnitude under identical conditions. Relative to biased WM, this approach achieves comparable sensitivity without requiring additional phase-bias compensation, substantially reducing system complexity and experimental overhead.

The remainder of this paper is organized as follows. Section 2 develops a theoretical framework for the proposed TS pointer based on spectral interference structures and derives its analytical relationship with the unknown time-delay parameter. Section 3 presents an experimental implementation using a broadband source and polarization interferometry, validating the TSWM scheme and quantitatively comparing its performance with that of the BWM approach. Section 4 systematically analyzes and compares the delay-measurement resolution limits of TSWM, conventional SWM, and BWM under identical detector-resolution constraints. Section 5 concludes the paper with a summary and outlook.

2. Theoretical Framework

Section 2 starts from the standard theoretical framework of SWM and introduces the BWM scheme as well as the proposed TSWM approach. A unified model is established to systematically compare the three methods in terms of sensitivity, dynamic range, and underlying physical mechanisms, thereby elucidating the origin of the performance advantages of the TSWM scheme; a schematic of WM is shown in Figure 1.

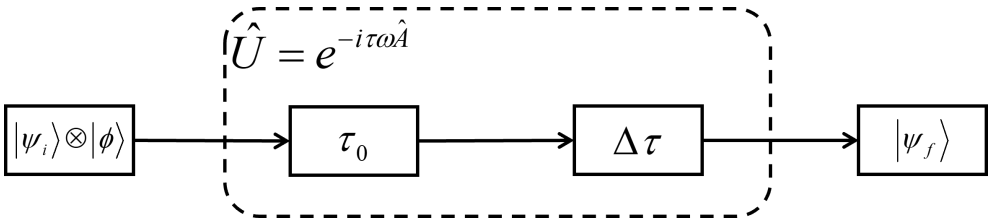


Figure 1. Schematic of a WM system, illustrating the three fundamental steps: preselection, weak interaction, and postselection.

Consider a prototypical WM system, where the system degree of freedom is encoded in the polarization state of a single photon. The system is initially prepared in the pre-selected state

$$|\psi_i\rangle = \frac{1}{\sqrt{2}}(|H\rangle + |V\rangle), \tag{1}$$

with $|H\rangle$ and $|V\rangle$ denoting the horizontal and vertical polarization states, respectively. The pointer is realized in the spectral degree of freedom of the photon, characterized by a Gaussian distribution centered at frequency ω_0 with spectral width σ:

$$|\phi\rangle = \int d\omega\, f(\omega)|\omega\rangle, \quad f(\omega) = \frac{1}{(2\pi\sigma^2)^{1/4}} \exp\left[-\frac{(\omega-\omega_0)^2}{4\sigma^2}\right], \tag{2}$$

where $|\omega\rangle$ represents the eigenstate of the frequency operator.

The weak interaction between the system and the pointer is implemented via a polarization-dependent time delay, which can be introduced by a birefringent element or an equivalent optical delay structure. The corresponding evolution operator is given by

$$\hat{U} = \exp(-i\tau\,\omega\,\hat{A}), \tag{3}$$

where $\hat{A} = |H\rangle\langle H| - |V\rangle\langle V|$ and τ denotes the effective time delay imparted by the system. In practical sensing scenarios, the total delay typically consists of a large fixed bias τ_0 and a small perturbation $\Delta\tau$ to be measured, i.e., $\tau = \tau_0 + \Delta\tau$, with the condition that $|\Delta\tau| \ll \tau_0$.

Under the weak coupling regime, the joint state of the system and the pointer evolves after the weak interaction as

$$|\Psi\rangle = \hat{U}(|\psi_i\rangle \otimes |\phi\rangle) = \frac{1}{\sqrt{2}} \int d\omega\, f(\omega) \left(e^{-i\omega\tau}|H\rangle + e^{i\omega\tau}|V\rangle \right) |\omega\rangle. \tag{4}$$

Subsequently, a post-selection is performed on the system by projecting it onto the state

$$|\psi_f\rangle = \frac{1}{\sqrt{2}} \left(e^{-i\varepsilon}|H\rangle - e^{i\varepsilon}|V\rangle \right), \tag{5}$$

where ε is the tunable post-selection angle. Upon successful post-selection, the pointer state collapses to

$$|\phi_f\rangle = \frac{1}{\sqrt{P_{\text{suss}}}} \langle \psi_f|\Psi\rangle = \frac{1}{\sqrt{P_{\text{suss}}}} \int d\omega\, f(\omega)[-i\, \sin(\omega\tau - \varepsilon)]|\omega\rangle, \tag{6}$$

where P_{suss} denotes the post-selection success probability, given by

$$P_{\text{suss}} = \left| \langle \psi_f|\Psi\rangle \right|^2 = \int d\omega\, f^2(\omega)\, \sin^2(\omega\tau - \varepsilon). \tag{7}$$

This result indicates that the post-selection interference modulates the original spectral distribution into an output exhibiting a periodic oscillatory structure, thereby providing a basis for constructing a novel pointer variable. Accordingly, the post-selected pointer spectral distribution can be expressed as

$$F(\omega) = \left| \langle \omega|\phi_f\rangle \right|^2 = \frac{P_0(\omega)}{P_{\text{suss}}}\, \sin^2(\omega\tau - \varepsilon), \tag{8}$$

where $P_0(\omega) = |\langle \omega|\phi\rangle|^2$ represents the probability distribution of the initial spectrum. This expression clearly shows that post-selection interference imprints a pronounced periodic modulation onto the original spectrum, establishing the physical foundation for defining a novel pointer variable.

In the SWM scheme, the mean shift in the output spectral distribution is typically chosen as the measurement pointer, which is expressed as

$$\delta\omega_{\text{SWM}} = \frac{\int_{-\infty}^{\infty} \omega P_0(\omega)\, d\omega}{\int_{-\infty}^{\infty} P_0(\omega)\, d\omega} - \omega_0 = \frac{2\sigma^2\tau\, e^{-\sigma^2\tau^2}\, \sin\left[2(\omega_0\tau - \varepsilon)\right]}{1 - e^{-\sigma^2\tau^2}\, \cos\left[2(\omega_0\tau - \varepsilon)\right]} \approx \frac{2\sigma^2\tau_{\text{SWM}}}{\varepsilon}, \tag{9}$$

where τ_{SWM} denotes the time delay (identical to τ in the exact expression, the subscript merely distinguishing the method), and the approximation is valid under the narrow condition $\omega_0\tau \ll \varepsilon \ll 1, \sigma^2\tau^2 \ll 1$.

Over a large time-delay range, the frequency shift exhibits both periodic and decaying behavior, as shown in Figure 2. The decay arises from the decoherence of orthogonal spectral components of a broadband source at large delays, which leads to a significant reduction in the sensing sensitivity as the delay increases.

It should be emphasized that the approximation in Equation (9) is valid only within a narrow parameter regime satisfying $\omega_0\tau \ll \varepsilon \ll 1$. Beyond this regime, the response of the mean pointer exhibits pronounced nonlinearity and may even show saturation or reversal, resulting in a measurement that is no longer monotonic or invertible. Under these conditions, the time-delay estimate is given by

$$\tau_{\text{SWM}} \approx \frac{\delta\omega_{\text{SWM}}}{2\sigma^2}\, \varepsilon. \tag{10}$$

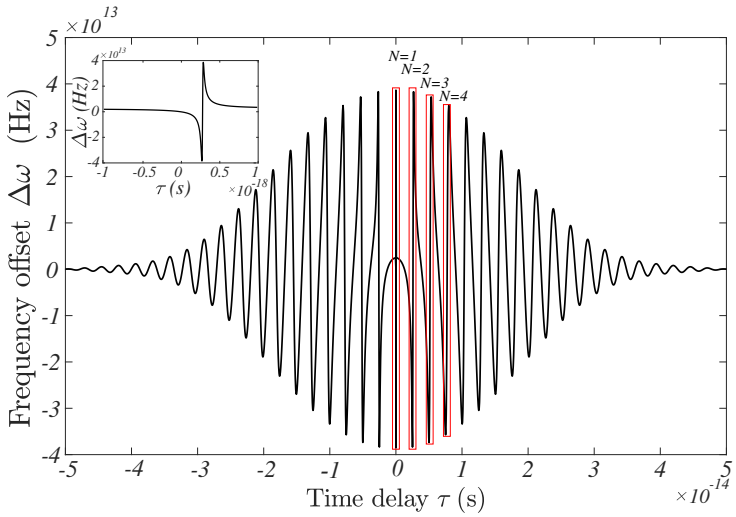


Figure 2. Variation in the frequency shift under the spectral pointer as a function of the time delay. The inset shows a magnified view of the sensing region for $N = 1$ on the attosecond scale.

To overcome the limited dynamic range and restricted sensing sensitivity inherent in the SWM scheme, the BWM approach introduces an additional phase bias τ_B in the presence of an initial delay τ_0. By selecting $\omega_0(\tau_0 + \tau_B) - \varepsilon = N\pi$ ($N = 0, 1, 2, \ldots$), the system operating point is locked near the linear region of the weak-value response, as indicated by the red-boxed area in Figure 2. This region exhibits extremely high sensitivity, albeit over a very narrow range. The corresponding mean shift is expressed as

$$\delta\omega_{\mathrm{BWM}} = \frac{2\sigma^2(\tau_0+\tau_B)\, e^{-\sigma^2(\tau_0+\tau_B)^2}\, \sin\left[2(\omega_0\tau + \omega_0(\tau_0+\tau_B) - \varepsilon)\right]}{1 - e^{-\sigma^2(\tau_0+\tau_B)^2}\, \cos\left[2(\omega_0\tau + \omega_0(\tau_0+\tau_B) - \varepsilon)\right]} \approx \frac{2\omega_0\tau_{\mathrm{BWM}}}{\tau_0+\tau_B}, \quad (11)$$

where the approximation holds under the condition $\omega_0\tau \ll \sigma\tau_0 \ll 1$, enabling a stable linear response under appropriate bias. Here, $\delta\omega_{\mathrm{BWM}}$ is the measured shift in the spectral mean induced by the time-delay τ_{BWM}. The corresponding time-delay estimate is then given by

$$\tau_{\mathrm{BWM}} \approx \frac{\delta\omega_{\mathrm{BWM}}}{2\omega_0}(\tau_0+\tau_B). \quad (12)$$

From a more fundamental perspective, both the SWM and BWM schemes rely solely on the first-order statistics (i.e., the mean) of the post-selected spectral distribution and thus fail to fully exploit the higher-order structural features inherent in the interference modulation process. Consequently, these approaches are inevitably constrained in practical applications by response saturation, periodic distortions, and a limited effective linear operating range, giving rise to an intrinsic trade-off between sensitivity enhancement and dynamic range extension.

To address these limitations, we propose and systematically investigate a TSWM scheme based on spectral structural features. Like conventional methods, TSWM employs a broadband spectral source as the initial pointer state; however, instead of using the spectral mean shift as the observable, TSWM directly utilizes the positions of the spectral extinction points formed by post-selection interference as the measurement pointer variable. This approach enables the simultaneous realization of high sensitivity and large dynamic range for phase or time-delay parameters within the weak measurement framework.

In the initial working state, no external perturbation is applied to the system, and the weak interaction stage involves only the intrinsic time delay τ_0 introduced by the birefringent medium. By adaptively tuning the post-selection angle ε, the output intensity

can be brought to a minimum $I_{\min}$ within a given interference period. At this point, the corresponding spectral dip is located at ω_{v0}, satisfying

$$\omega_{v0}\tau_0 - \varepsilon_0 = N\pi, \tag{13}$$

where $N = 0, 1, 2, \ldots$ denotes the interference period of the system, uniquely determined by the known initial delay τ_0. Unlike the spectral mean, the positions of these dips are dictated by the interference condition for destructive superposition, exhibiting extremely high contrast and stable identifiability, thereby providing a solid physical foundation for constructing high-precision pointer variables.

Under the aforementioned working-point condition, when an external perturbation induces a change in the total time delay $\Delta\tau$, the post-selected spectral distribution undergoes a corresponding overall shift, with the position of the spectral dip moving by $\Delta\omega$, satisfying

$$(\omega_{v0} + \Delta\omega)(\tau_0 + \Delta\tau) - \varepsilon_0 = N\pi. \tag{14}$$

Under the condition that the product $\Delta\omega\Delta\tau$ is negligible, this relationship establishes a one-to-one correspondence between the perturbation-induced time-delay change $\Delta\tau$ and the spectral dip shift $\Delta\omega$, given by

$$\Delta\tau_{\mathrm{TSWM}} = -\frac{\Delta\omega}{\omega_{v0}}\,\tau_0. \tag{15}$$

Unlike conventional spectral interferometry, where dip shifts originate purely from classical optical path differences, the trough shift in TSWM arises from the weak-value amplification mechanism within the framework of quantum weak measurement. The spectral interference here is not merely a classical fringe but a result of specific pre- and post-selection on photonic states, where the zero-intensity point serves as an amplified pointer with its shift analytically linked to the weak value.

Equation (13) clearly indicates that, in the TSWM scheme, the interference period N is determined solely by the initial delay τ_0, and for perturbations satisfying $\Delta\tau \ll \tau_0$, the system's dynamic range within a single period is not significantly extended. Nevertheless, compared to the BWM approach, TSWM does not require an additional phase-biasing device, thereby substantially reducing system complexity and experimental implementation costs.

To further enable multi-period and large dynamic-range measurements of phase and time delay, the TSWM scheme implements a two-step post-selection adjustment process to extract the interference-period information of the system.

First, the post-selection tuning is performed. Initially, the phase satisfies the condition $\omega_{v0}\tau_0 - \varepsilon_0 = N\pi$, where the intrinsic delay τ_0 and the corresponding interference period N are unknown, and the target time delay is $\tau = \tau_0 + \Delta\tau$. By finely adjusting the post-selection angle by $\Delta\varepsilon$, such that $\varepsilon = \varepsilon_0 + \Delta\varepsilon$, the shifted spectral dip occurs at a frequency ω_{v1} satisfying

$$\omega_{v1}\tau_0 - (\varepsilon_0 + \Delta\varepsilon) = N\pi. \tag{16}$$

Here, the dip frequency can be expressed as $\omega_{v1} = \omega_{v0} + \Delta\omega_v$, with $\Delta\omega_v$ denoting the corresponding dip shift.

Subsequently, the period of the target phase signal can be extracted. With the post-selection angles ε and $\Delta\varepsilon$ known, the shifted spectral dip frequency ω_{v1} can be measured, yielding

$$N\pi = \frac{\Delta\varepsilon}{\Delta\omega_v}\,\omega_{v0} - \varepsilon_0, \tag{17}$$

which uniquely determines the previously unknown large time delay τ_0 and its corresponding interference period N. Once the period information is obtained, the local linear region within any interference period can be selected for precision measurement, thereby

overcoming the limitation of conventional mean-pointer methods that are restricted to a single linear interval and enabling true large-dynamic-range parameter estimation.

Since the spectral dips repeat periodically with a fixed spacing, identifying the integer order N of the current dip allows a unified parameter inversion to be established across multiple interference periods. This effectively eliminates ambiguities and uncertainties arising from the periodic response in conventional weak measurement schemes. Consequently, the dip-shift pointer structurally overcomes the fundamental limitation of mean-pointer methods confined to single-period linear operation, providing a new design paradigm for weak measurement systems that simultaneously achieve high sensitivity and large dynamic range.

Moreover, because the dip positions are determined by interference zeros, they exhibit intrinsic robustness against overall intensity fluctuations, source power noise, and certain spectral distortions. As long as the system visibility remains above the identifiable threshold, the dip positions can be stably extracted. Therefore, this approach is applicable not only to ideal Gaussian spectral sources but also to practical broadband non-Gaussian sources and complex spectral environments, significantly enhancing its engineering adaptability and implementation flexibility in optical metrology and sensing applications.

3. Experimental Implementation

To validate the practical performance of the TSWM scheme, we constructed an experimental setup based on a broadband light source and polarization modulation. The overall system layout is shown in Figure 3, where the core components work in concert to enable precise time-delay sensing.

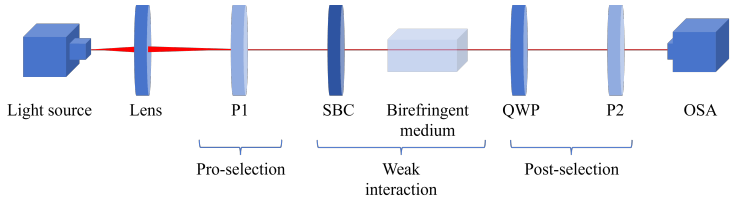


Figure 3. Schematic diagram of the experimental setup for the Trough-shift pointer for weak measurement scheme. Light source: broad spectrum light source; P1, P2: polarizer; QWP: quarter-wave plate; SBC: Soleil-Babinet compensator; Birefringent medium: sample to be measured; OSA: spectrometer.

The experiment employs a broadband amplified spontaneous emission source (ASE730, Thorlabs, Newton, NJ, USA) with an emission spectrum in the C–L band and a spectral width of approximately 30 nm. The initial spectral distribution is shown as the red solid line in Figure 4. The output from the source is first collimated into a parallel beam using a collimating lens and then directed into the pre-selection polarization modulation module. This module employs a polarizer P1 with a fixed transmission axis at 45°, which prepares the input unpolarized light into the pre-selected state $|\psi_i\rangle$.

During the weak interaction stage, a Soleil–Babinet compensator (SBC) is introduced as a controllable phase-delay element, producing a wavelength-dependent phase shift expressed as

$$\phi(\lambda) = \frac{2\pi}{\lambda}\Delta n \cdot d, \tag{18}$$

where Δn is the birefringence and d is the thickness difference of the compensator. By precisely adjusting the SBC, a known initial time delay τ_0 can be introduced into the system, followed by the birefringent crystal generating the target delay $\Delta\tau$.

The post-selection is implemented using a polarizer P2 in combination with a quarter-wave plate (QWP), with the transmission axis set at $-45° - \varepsilon$, where ε is the tunable post-selection angle for accurate preparation of the post-selected state $|\psi_f\rangle$. The final

output is recorded by a high-resolution optical spectrum analyzer (AQ6370D, Yokogawa, Tokyo, Japan) with a frequency resolution of $\Delta\Omega = 1 \times 10^9$ rad/s, enabling precise acquisition of the post-selected spectral distribution. The colored solid lines in Figure 4 show the measured output spectra under different small phase perturbations introduced by the SBC.

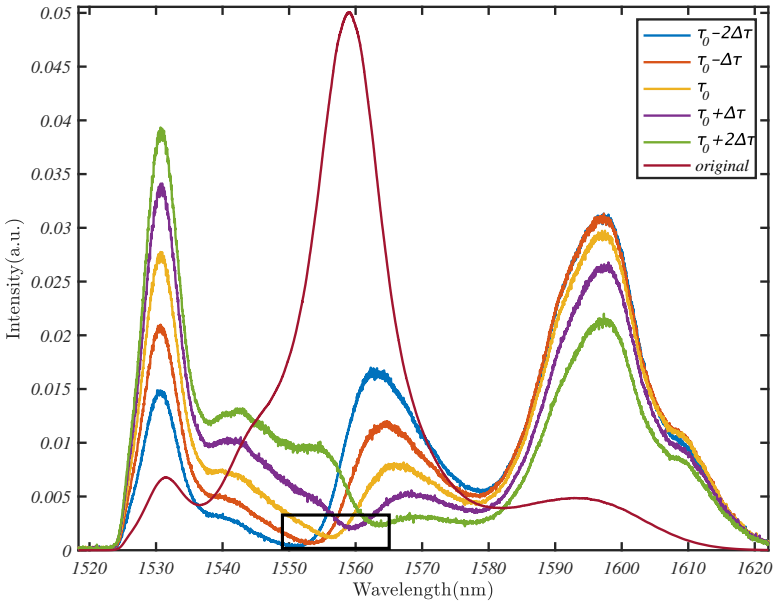


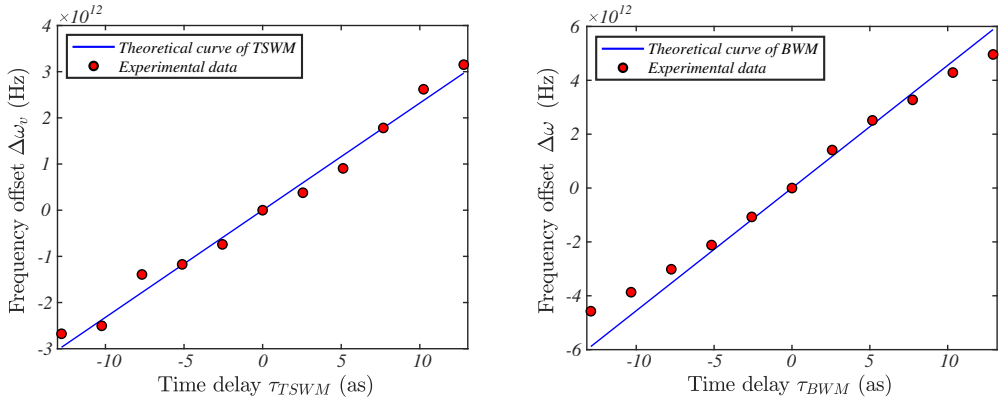
Figure 4. Initial spectral distribution of the light source and the spectral dip shifts observed during the weak measurement process, where a SBC is used to simulate time-delay variations. In the figure, the initial delay is $\tau_0 = 5.2392 \times 10^{-15}$ s, and each curve corresponds to a time-delay shift of $\Delta\tau = 1.7984 \times 10^{-17}$ s.

In these spectra, the three weak-measurement methods correspond to distinct features. For TSWM, the measurement pointer is the spectral position of the extinction dip. The black rectangle near 1560 nm indicates the region of interest where the dip is located and tracked. For SWM and BWM, the pointer is the centroid (mean wavelength) of the entire spectrum, obtained by numerical integration over all wavelengths. It can be seen that, despite deviations of the initial spectrum from an ideal Gaussian shape, the post-selection interference produces clearly resolved double-peak structures and well-defined extinction dips, with the experimental results in good agreement with theoretical simulations.

These results indicate that the dip-shift pointer does not rely on a strict Gaussian spectral distribution but only requires sufficient interference visibility. Consequently, the method maintains good applicability under practical broadband light sources and complex spectral profiles, providing a solid experimental foundation for its deployment in engineered sensing systems.

To further evaluate the performance of the TSWM scheme in terms of sensitivity and linear response, we selected a specific spectral dip as the reference point and recorded its initial frequency position ω_{v0}. The SBC was then gradually adjusted to introduce small phase perturbations, while the corresponding shift in the dip frequency $\Delta\omega_v$ was measured in real time. The experimental results are shown in Figure 5a. Over a relatively wide perturbation range, the dip-frequency shift exhibits a linear relationship with the phase perturbation, in good agreement with the theoretical prediction given by Equation (9), thereby validating the effectiveness and stability of the dip-shift pointer as a weak-measurement readout.

For comparison, the BWM scheme was also tested experimentally. In this case, an additional phase bias was introduced to lock the system within the linear region of the mean-response, and the change in the spectral mean with respect to phase perturbation was measured. The results are presented in Figure 5b.



(**a**) (**b**)

Figure 5. Spectraldip shifts observed during the weak measurement process with phase changes simulated using a SBC. (**a**) corresponds to the TSWM scheme. (**b**) shows the BWM scheme with an additional phase bias. The absolute values of the shifts are plotted to ensure positive slopes for both schemes, facilitating resolution comparison.

From the experimental results, both TSWM and BWM schemes demonstrate comparable measurement sensitivity. However, TSWM exhibits a higher degree of agreement with theoretical predictions and achieves a stable linear response without the need for an additional biasing element, highlighting its overall advantages in system complexity, stability, and practical implementability.

For time-delay estimation, the sensitivity is defined as the ratio between the change in the observable and the corresponding change in the parameter of interest, i.e.,

$$S = \left|\frac{\Delta\omega}{\Delta\tau}\right| = \frac{4\pi^2 c^2}{\lambda^3}\left|\frac{\Delta\lambda}{\Delta\phi}\right|, \tag{19}$$

where $\Delta\omega$ denotes the shift in the spectral feature (dip) and $\Delta\tau$ represents the corresponding change in the time delay. Within the linear operational range of the experiment, $\Delta\omega$ varies linearly with $\Delta\tau$, so the sensitivity S corresponds to the slope of the fitted line, with physical units of $\mathrm{rad/s^2}$.

Linear fitting of the experimental data yields the sensitivities for TSWM and BWM as

$$S^{\mathrm{exp}}_{\mathrm{TSWM}} = 2.289 \times 10^{29}\ \mathrm{rad/s^2} = 244.9\ \mathrm{nm/rad}, \tag{20}$$

$$S^{\mathrm{exp}}_{\mathrm{BWM}} = 3.904 \times 10^{29}\ \mathrm{rad/s^2} = 417.7\ \mathrm{nm/rad}, \tag{21}$$

while the corresponding theoretical predictions are

$$S^{\mathrm{th}}_{\mathrm{TSWM}} = 2.320 \times 10^{29}\ \mathrm{rad/s^2} = 248.2\ \mathrm{nm/rad}, \tag{22}$$

$$S^{\mathrm{th}}_{\mathrm{BWM}} = 4.556 \times 10^{29}\ \mathrm{rad/s^2} = 487.5\ \mathrm{nm/rad}. \tag{23}$$

It can be seen that the relative deviation between the experimental and theoretical sensitivities for TSWM is approximately 1.3%, significantly smaller than the ∼14.3% deviation observed for the BWM scheme. This indicates that TSWM exhibits stronger robustness to model assumptions and device imperfections, and its response characteristics more closely approach the ideal theoretical model in practical implementations.

The experimental uncertainty primarily arises from the following factors: (i) the limited resolution of the optical spectrum analyzer and pixel sampling noise, which constrain the precision of dip-position extraction; (ii) deviations in the post-selected state induced by polarizer angle drifts and waveplate phase-delay errors; and (iii) fluctuations in source power and spectral shape, which affect the interference visibility. Since the TSWM scheme relies directly on the positions of interference zeros rather than overall intensity or mean

statistics, it exhibits inherent robustness against power fluctuations and spectral distortions, a feature confirmed by repeated measurements.

Taken together, these results indicate that although the BWM scheme possesses a higher theoretical sensitivity limit under ideal conditions, TSWM achieves comparable measurement performance without requiring additional biasing elements. Moreover, TSWM demonstrates superior consistency, stability, and practical implementability, providing a more practically viable paradigm for high-precision weak-measurement-based optical sensing.

4. Resolution Analysis

To quantitatively evaluate the performance advantage of the proposed TSWM scheme, we conduct a systematic comparison of the ultimate resolution limits of the SWM, BWM, and TSWM schemes under identical instrumentation conditions. To highlight the intrinsic performance differences stemming from the pointer mechanisms themselves, the analysis considers only the finite frequency resolution $\Delta\Omega$ of the optical spectrum analyzer as the dominant source of measurement uncertainty while neglecting other non-ideal factors such as source intensity noise, detection noise, and statistical fluctuations.

In the SWM scheme, the mean shift in the output spectral distribution serves as the measurement pointer. From the theoretical model presented above, the corresponding limit of resolvable longitudinal phase shift satisfies

$$\varphi_{\mathrm{SWM}} = 2\omega_0\tau_{\mathrm{SWM}} \geq \frac{\omega_0\Delta\Omega}{\sigma^2}\varepsilon. \tag{24}$$

This expression indicates that the minimum resolvable phase shift in SWM not only is constrained by the spectrometer resolution $\Delta\Omega$ but also strongly depends on the post-selection angle ε and the pointer spectral width σ. Moreover, due to the effective linear response range being limited to regions near the weak-value singularity, when ε is too small, the system may enter a saturated or non-monotonic regime, making it difficult in practice to simultaneously achieve high sensitivity and a large dynamic range.

In the BWM scheme, by introducing an additional bias phase τ_0 and locking the system near the linear region of the weak-value response, the dynamic range limitation inherent to SWM can be partially alleviated. The corresponding limit of resolvable longitudinal phase shift is given by

$$\varphi_{\mathrm{BWM}} = 2\omega_0\tau_{\mathrm{BWM}} \geq \frac{\Delta\Omega}{\omega_0}\varepsilon. \tag{25}$$

Compared with SWM, the BWM resolution expression no longer explicitly depends on the pointer spectral width σ, providing greater flexibility in parameter design. However, this scheme relies on precise tuning and long-term stabilization of the additional bias phase element, often requiring extra compensation modules or active feedback systems, which increases system complexity and experimental implementation difficulty.

In the TSWM scheme, the measurement pointer is constituted by the positions of structurally defined dips in the post-selected spectral distribution, rather than by its mean statistics. According to the theoretical derivation above, when selecting the lowest-order dip ($N = 0$), the corresponding limit of resolvable longitudinal phase shift satisfies

$$\varphi_{\mathrm{TSWM}} = 2\omega_{v0}\Delta\tau_{\mathrm{TSWM}} \geq \frac{2\Delta\Omega}{\omega_{v0}}\varepsilon_0. \tag{26}$$

This result indicates that the TSWM resolution is primarily determined by the reference frequency ω_{v0} associated with the dip and the post-selection angle ε_0, without relying on weak-value singularity amplification or additional bias-phase modulation. Since the dip positions are dictated by interference null conditions, the response maintains a strictly linear relation with parameter variations and is immune to saturation or periodic distortions that

affect mean-value pointers over a large parameter range. Consequently, TSWM significantly extends the measurable dynamic range while preserving high sensitivity.

The above results indicate that, under identical spectrometer resolution, the TSWM scheme achieves phase-resolving capability comparable to that of BWM, without relying on weak-value singularity amplification or additional bias-phase modulation, and significantly outperforms the conventional SWM scheme. The minimum resolvable phase shift can reach the order of 10^{-7} while avoiding the saturation issues commonly encountered in mean-value pointer mechanisms operating in high-gain regions.

Further numerical simulations are shown in Figure 6. The longitudinal phase shift resolution R for all three schemes exhibits a strict inverse proportionality to the spectrometer resolution $\Delta\Omega$, appearing as straight lines with identical negative slopes on a logarithmic scale. This indicates that all three methods are fundamentally constrained by the same instrumental noise floor and that the performance differences primarily arise from the distinct response mechanisms of the chosen pointer variables to parameter variations.

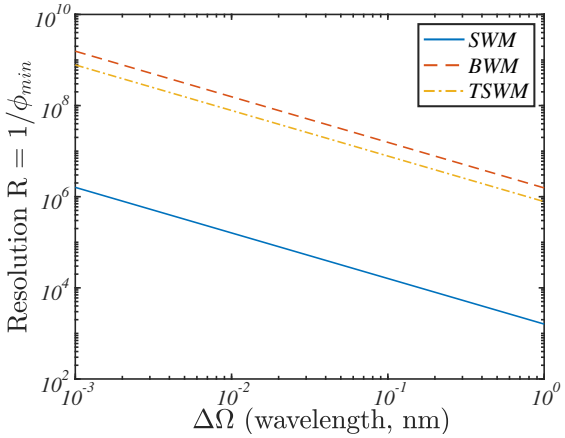


Figure 6. Ultimate system resolution limits of SWM, BWM, and TSWM under spectrometer resolution-limited conditions.

Specifically, the BWM scheme exhibits the highest resolution, approximately 1.56×10^8; TSWM follows, around 7.8×10^7, roughly half that of BWM; and SWM has the lowest resolution, only 1.6×10^5, about three orders of magnitude lower than that of TSWM. These results clearly demonstrate that TSWM achieves near-optimal measurement precision while maintaining a simplified system architecture, significantly extending the dynamic range, and thus provides a practical and robust route for the engineering application of weak measurements in high-precision optical metrology and sensing.

5. Conclusions

In summary, we propose and experimentally demonstrate a novel WM scheme based on spectral structural features—TSWM. Unlike conventional SWM or BWM, which employ the spectral mean as the pointer, TSWM utilizes the positions of spectral extinction points induced by post-selection interference to encode the phase or time-delay information, simultaneously achieving high sensitivity and large dynamic range. Unified theoretical analysis of SWM, BWM, and TSWM shows that, under identical instrumental resolution, TSWM significantly outperforms SWM and attains resolution comparable to BWM while avoiding saturation and periodic distortion associated with mean-value pointers. Experimentally, TSWM demonstrates robust, linear valley-shift responses even under non-ideal broadband spectral conditions, simplifying system complexity compared with BWM. These results highlight that optimal pointer variables in weak measurements can extend beyond first-order statistics to structural features of the distribution, providing a practical and

robust paradigm for high-precision, large-dynamic-range optical metrology and sensing. Owing to these advantages, the proposed TSWM scheme holds promise for a variety of precision measurement scenarios that demand both ultra-high sensitivity and a broad operational range, such as stress measurement and biosensing.

Author Contributions: Conceptualization, W.H.; methodology, W.H. and Z.S.; investigation, W.H. and Z.S.; software , W.Z.; writing—original draft preparation, W.H., Z.S. and W.Z.; writing—review and editing, J.W., Y.Y. and Z.W.; funding acquisition, J.W., Y.Y. and Z.W. All authors have read and agreed to the published version of the manuscript.

Funding: This research was funded by the Innovation Program for Quantum Science and Technology (2021ZD0300701), the National Natural Science Foundation of China (62371199, 62071186, 61771205), the Natural Science Foundation of Guangdong Province (2024A1515012427), Guangdong Provincial Quantum Science Strategic Initiative(GDZX2305001) and the Guangdong Provincial Key Laboratory (2020B1212060066).

Data Availability Statement: The datasets generated and/or analyzed during the current study are available from the corresponding author on reasonable request. Experimental spectral measurements and numerical simulation data supporting the findings of this study are not publicly deposited due to the large file size and ongoing related experiments but can be provided upon request. No data involving human or animal subjects were used in this study.

Conflicts of Interest: The authors declare no conflicts of interest.

References

1. Aharonov, Y.; Albert, D.Z.; Vaidman, L. How the result of a measurement of a component of the spin of a spin-1/2 particle can turn out to be 100. *Phys. Rev. Lett.* **1988**, *60*, 1351. [CrossRef]
2. Dressel, J.; Malik, M.; Miatto, F.M.; Jordan, A.N.; Boyd, R.W. Colloquium: Understanding quantum weak values: Basics and applications. *Rev. Mod. Phys.* **2014**, *86*, 307–316. [CrossRef]
3. Wang, G.; Li, H.; Xiao, T.; Huang, J.; Zeng, G. Adaptive correction of phase estimation with time based on weak measurement. *Opt. Express* **2021**, *29*, 39150–39158. [CrossRef] [PubMed]
4. Li, H.; Wang, G.; Xia, B.; Song, Q.; Huang, J.; Zeng, G. High precision phase estimation with controllable sensitivity and dynamic range. *J. Phys. At. Mol. Opt. Phys.* **2021**, *54*, 215503. [CrossRef]
5. Zhao, W.Q.; Pang, S.N.; Su, Z.F.; Zhao, T.M.; Wang, J.D.; Yu, Y.F. Rigorous verification of quantum contextuality from anomalous weak value. *Chin. Phys. B* **2026**, *35*, 020301. [CrossRef]
6. Zhao, W.Q.; Su, Z.F.; Yu, Y.F.; Wang, J.D. Long-Distance High-Precision and High-Sensitivity Time Delay Variation Sensing Based on Fiber-Optic Weak Measurements. *J. Light. Technol.* **2025**, *43*, 6948–6956. [CrossRef]
7. Li, C.F.; Xu, X.Y.; Tang, J.S.; Xu, J.S.; Guo, G.C. Ultrasensitive phase estimation with white light. *Phys. Rev. A* **2011**, *83*, 044102. [CrossRef]
8. Xu, X.Y.; Kedem, Y.; Sun, K.; Vaidman, L.; Li, C.F.; Guo, G.C. Phase estimation with weak measurement using a white light source. *Phys. Rev. Lett.* **2013**, *111*, 033604. [CrossRef]
9. Xu, K.; Hu, X.M.; Hu, M.J.; Wang, N.N.; Zhang, C.; Huang, Y.F.; Liu, B.H.; Li, C.F.; Guo, G.C.; Zhang, Y.S. Measuring small longitudinal phase shifts via weak measurement amplification. *Chin. Phys. B* **2024**, *33*, 030602. [CrossRef]
10. Luo, Z.; Wu, H.; Xu, L.; Chang, T.; Wu, P.; Du, C.; Cui, H.L. Phase measurement of optical fiber via weak-value amplification. *IEEE Sens. J.* **2019**, *19*, 6742–6747. [CrossRef]
11. Brunner, N.; Scarani, V.; Wegmüller, M.; Legré, M.; Gisin, N. Direct measurement of superluminal group velocity and signal velocity in an optical fiber. *Phys. Rev. Lett.* **2004**, *93*, 203902. [CrossRef]
12. Brunner, N.; Acín, A.; Collins, D.; Gisin, N.; Scarani, V. Optical Telecom Networks as Weak Quantum Measurements with Postselection. *Phys. Rev. Lett.* **2003**, *91*, 180402. [CrossRef]
13. Dixon, P.B.; Starling, D.J.; Jordan, A.N.; Howell, J.C. Ultrasensitive beam deflection measurement via interferometric weak value amplification. *Phys. Rev. Lett.* **2009**, *102*, 173601. [CrossRef]
14. Zhang, C.; Lai, Y.; Yang, R.; Liu, K.; Zhang, J.; Sun, H.; Gao, J. Small-tilt measurement based on weak-value-amplification with balanced homodyne detection. *Appl. Phys. Lett.* **2023**, *122*, 031107. [CrossRef]
15. Hosten, O.; Kwiat, P. Observation of the spin Hall effect of light via weak measurements. *Science* **2008**, *319*, 787–790. [CrossRef] [PubMed]

16. Luo, Z.; Huang, J.; Song, Q.; Xia, B.; Li, H.; Zeng, G. High-sensitivity and wide-dynamic-range parameter estimation via weak-value amplification. *Phys. Rev. Appl.* **2024**, *22*, 064070. [CrossRef]
17. Luo, L.; Xie, L.; Qiu, J.; Zhou, X.; Liu, X.; Li, Z.; He, Y.; Zhang, Z.; Sun, H. Simultaneously precise estimations of phase and amplitude variations based on weak-value amplification. *Appl. Phys. Lett.* **2019**, *114*, 111104. [CrossRef]
18. Yin, P.; Zhang, W.H.; Xu, L.; Liu, Z.G.; Zhuang, W.F.; Chen, L.; Gong, M.; Ma, Y.; Peng, X.X.; Li, G.C.; et al. Improving the precision of optical metrology by detecting fewer photons with biased weak measurement. *Light. Sci. Appl.* **2021**, *10*, 103. [CrossRef]
19. Zhang, Z.H.; Chen, G.; Xu, X.Y.; Tang, J.S.; Zhang, W.H.; Han, Y.J.; Li, C.F.; Guo, G.C. Ultrasensitive biased weak measurement for longitudinal phase estimation. *Phys. Rev. A* **2016**, *94*, 053843. [CrossRef]
20. Song, Q.; Li, H.; Huang, J.; Xiao, T.; Tan, X.; Xia, B.; Zeng, G. Adaptive time-varying parameter estimation via weak measurement. *Phys. Rev. Appl.* **2022**, *18*, 044031. [CrossRef]
21. Li, D.; Cai, G.; Song, C.; Weng, C.; Chen, C.; Zheng, W.; Zhang, Y.; Li, K. Polarization beam splitting in a Glan-Taylor prism based on dual effects of both birefringence and Goos-Hanchen shift. *Heliyon* **2022**, *8*, e11754. [CrossRef] [PubMed]
22. Xu, L.; Luo, L.; Wu, H.; Luo, Z.; Zhang, Z.; Shi, H.; Chang, T.; Wu, P.; Du, C.; Cui, H.L. Measurement of chiral molecular parameters based on a combination of surface plasmon resonance and weak value amplification. *ACS Sens.* **2020**, *5*, 2398–2407. [CrossRef] [PubMed]

Disclaimer/Publisher's Note: The statements, opinions and data contained in all publications are solely those of the individual author(s) and contributor(s) and not of MDPI and/or the editor(s). MDPI and/or the editor(s) disclaim responsibility for any injury to people or property resulting from any ideas, methods, instructions or products referred to in the content.